ADVANCED HEALTHCARE MATERIALS
www.advhealthmat.de

Directing Stem Cell Differentiation by Changing the Molecular Mobility of Supramolecular Surfaces

*Ji-Hun Seo, Sachiro Kakinoki, Tetsuji Yamaoka, and Nobuhiko Yui**

Mesenchymal stem cells (MSCs) are multipotent cells that can differentiate into various types of cells, such as adipogenic, myogenic, chondrogenic, and osteogenic cells.[1] Communication with contacted materials determines the physiological activity of cells; therefore, regulating MSC fate by controlling the physicochemical properties of cell-contacting materials is an important issue in the field of biomaterials.[2] One representative series of studies relies on the effect of material stiffness on MSC lineage. MSCs that adhere to stiff elastomer surfaces reveal a well-spread and polarized morphology with mature actin fibers, resulting in the differentiation of the adherent stem cells into osteogenic cells rather than myogenic or adipogenic cells.[3] By contrast, MSCs on a soft surface demonstrate limited spreading and a round morphology with immature actin fibers, resulting in better differentiation into adipo- or myogenic cells.[4] A similar tendency has also been reported when other types of mechanostresses (e.g., shear stress, hydrostatic pressure, topographical stress, and degradation stress) were administered to cells using various 2- and 3D materials, such as flow channels, cross-linked elastomers, micropatterned surfaces, and hydrogels.[5] Although the design methodologies of these materials differ, these results reveal a consistent phenomenon in which stem cell differentiation is greatly dominated by the cytoskeleton that forms when the cells are grown on or in the artificial materials. From these perspectives, we hypothesized that a simple surface treatment (e.g., polymer casting or dip coating) of materials that is capable of changing the adhesion morphology of cells would be a useful way to induce a specific type of differentiation of adherent stem cells. This treatment could provide an attractive method of directly inducing differentiation into a desired type of stem cells on various types of biomedical devices that could be used in vivo or in vitro without changing the bulk properties of the materials. The underlying concept that we applied is modulating the morphology of adhering stem cells by changing the molecular mobility of deposited polymer surface. Because cells determine the physiological activity by dynamic interaction with materials surfaces, difference in molecular mobility of cell-contacting polymer surface is anticipated to enable the regulation of cell function. To this end, designing a molecular platform capable of developing wide range of molecular mobility when hydrated was necessary.

Polyrotaxane (PRX) is a supermolecule that contains molecularly movable host molecules [e.g., α-cyclodextrin (α-CD)] threaded on a linear guest molecule [e.g., poly(ethylene glycol) (PEG)]. Previously, we reported that this PRX molecule could be stably deposited on material surfaces by introducing surface-anchoring groups at both ends of the PRX segment and that this type of threaded macromolecular surface shows high surface mobility in the hydrated state comparing to the conventional methacrylate polymers.[6] Introducing a hydrophobic methoxy group or arginine-glycine-aspartate (RGD) peptide sequence on threaded α-CD molecules created cell-adherent PRX surfaces.[7] Interestingly, mouse fibroblasts that adhered to the PRX block copolymer surfaces with high molecular mobility show a protruded and elongated morphology in contrast to their wide and spread morphology on conventional methacrylate copolymer surfaces.[7a] Moreover, human umbilical vein endothelial cells (HUVECs) on the PRX block copolymer surfaces show a disrupted and immature actin fiber orientation, whereas the cells grown on other cell adhesive surfaces with lower surface mobility show an obvious and mature actin fiber orientation.[8] These results suggest that a simple deposition of PRX block copolymers on material surfaces could induce different cell responses and presumably the differentiation of MSCs.

Figures 1a and S1 (Supporting Information) show the molecular structures of the PRX block and the control random copolymers with the overall method of surface preparation. PRX-A1 is a block copolymer containing 12 threaded α-CD molecules on PEG (molecular weight: 20000). PRX-B1 contains 123 threaded α-CD molecules with a weight percent of hydrophobic methoxy groups (OMe, below 10 wt%) on α-CD that is similar to that for PRX-A1. PRX-B2 contains 104 threaded α-CD molecules, which is a similar number but higher weight percent of OMe groups than that of PRX-B1. Because the synthesized PRX block copolymers contained four chemical groups (i.e., phosphorylcholine and *n*-butyl groups in the anchoring groups and hydroxyl and OMe groups on the α-CD molecules) with a methacrylate/PEG backbone, the corresponding random copolymers containing the same chemical groups were also prepared (Table S1, Supporting Information).

The prepared polymers were deposited on glass surface, and the surface-free energy was calculated based on Owens-Wendt plots using the contact angles of methylene iodide and an air bubble in water as the non-polar and polar components, respectively.[7a] The surface-free energy, which is roughly described using the term "polarity" ("hydrophobicity" or "hydrophilicity"), is an important factor for characterizing

Dr. J.-H. Seo, Dr. S. Kakinoki, Dr. T. Yamaoka, Prof. N. Yui
JST-CREST, Tokyo 102–0076, Japan
E-mail: yui.org@tmd.ac.jp
Dr. J.-H. Seo, Prof. N. Yui
Institute of Biomaterials and Bioengineering
Tokyo Medical and Dental University
2–3–10 Kanda-Surugadai, Chiyoda, Tokyo 101–0062, Japan
Dr. S. Kakinoki, Dr. T. Yamaoka
Department of Biomedical Engineering
National Cerebral and Cardiovascular Center Research Institute
Suita, Osaka 565–8565, Japan

DOI: 10.1002/adhm.201400173

ADVANCED HEALTHCARE MATERIALS
www.advhealthmat.de

www.MaterialsViews.com

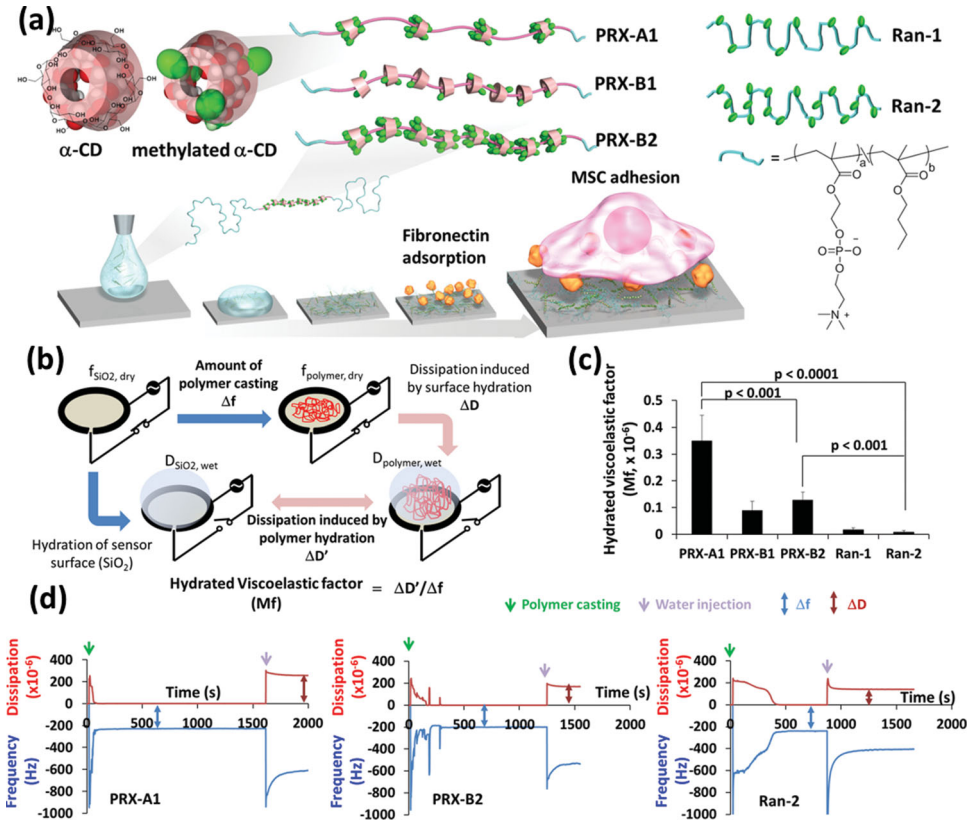

Figure 1. Concept of PRX block copolymers and the schematic explanation of measuring hydrated viscoelastic factor (Mf). a) Molecular structure of PRX block copolymers and the overall polymer deposition scheme. b) The overall measuring process of Mf. c) The results of Mf on the polymer surfaces. Data are presented as mean ± s.d. ($n = 4$). d) The results of monitoring the polymer deposition and hydration on the PRX-A1, PRX-B2, and the Ran-2 surface using the QCM-D equipment. The results for PRX-B1 and Ran-1 are presented in the Supporting Information.

biomaterial surfaces.[9] However, all the prepared polymer surfaces in this study demonstrated hydrophilic properties, that is, approximately 65 mJ m^{-2} of surface-free energy (Table S2, Supporting Information), which is higher than that of poly(2-hydroxyethyl methacrylate) surface:a conventional hydrophilic polymer.[10] Therefore, the concept of the term "polarity," could not be applied to discuss the different responses of MSCs to the polymer surfaces. The molecular mobility of the polymer surfaces when hydrated (Mf) were estimated by quartz crystal microbalance with dissipation (QCM-D) analysis (Figure 1b). QCM-D analysis has been widely used to measure polymer mobility, in terms of viscoelasticity, on the outermost surface in aqueous media.[11] The clear differences in Mf values were observed between the PRX block copolymer surfaces (10- or 20-fold higher) and the random copolymer surfaces, and significant differences were even observed between the PRX-A and B surfaces (Figure 1c). The decrease in the Mf on the PRX-B surface relative to that on the PRX-A1 surface may be due to an increased rigidity or decreased molecular mobility that is induced by the 10-fold higher number of threaded α-CD molecules in the PRX-B surface.[12] This increased rigidity may induce the less-swelled state of the polymer surface in hydrated states, thus provide lower value of Mf. In any event, this indicates that a series of PRX block copolymers is a useful molecular platform for regulating Mf values by simply changing the number of threaded α-CD molecules.

Figures 2a and S3 (Supporting Information) show the morphologies of the adherent MSCs after 4 d of incubation in a non-differentiation medium. To investigate the polymer–MSC interaction without other factors (e.g., changes in physiological activity due to the differentiation process, including morphological changes),[13] the MSC response on the prepared polymer surfaces was estimated in non-differentiation states. Overall, the MSCs on the dynamic PRX block copolymer surfaces revealed a narrow, protruded and elongated morphology (Figure S3, Supporting Information) with relatively immature actin fiber orientation, whereas broad and spread morphologies with relatively matured actin fiber bundles were observed on the random copolymer surfaces after 4 d. The morphological characteristics, specifically the aspect ratio and the cell area, were quantitatively analyzed using ImageJ software. This analysis revealed that the MSCs on the PRX surfaces with higher Mf showed morphologies with greater elongation (lower aspect ratio, Figure S5, Supporting Information) than that of MSCs on the random copolymer surfaces with lower Mf. Although more clear morphological differences were observed at the early stage of MSCs adhesion (4 h, Figure S4, Supporting Information), weak MSCs adhesion on the PRX-B1 and Ran-1 surfaces precludes us conducting a quantitative analysis of the adhering morphologies of MSCs. In any event, it was confirmed that a significant difference in morphology of adhering MSCs could be induced by altering the molecular mobility.

DOI: 10.1002/adhm.201400173

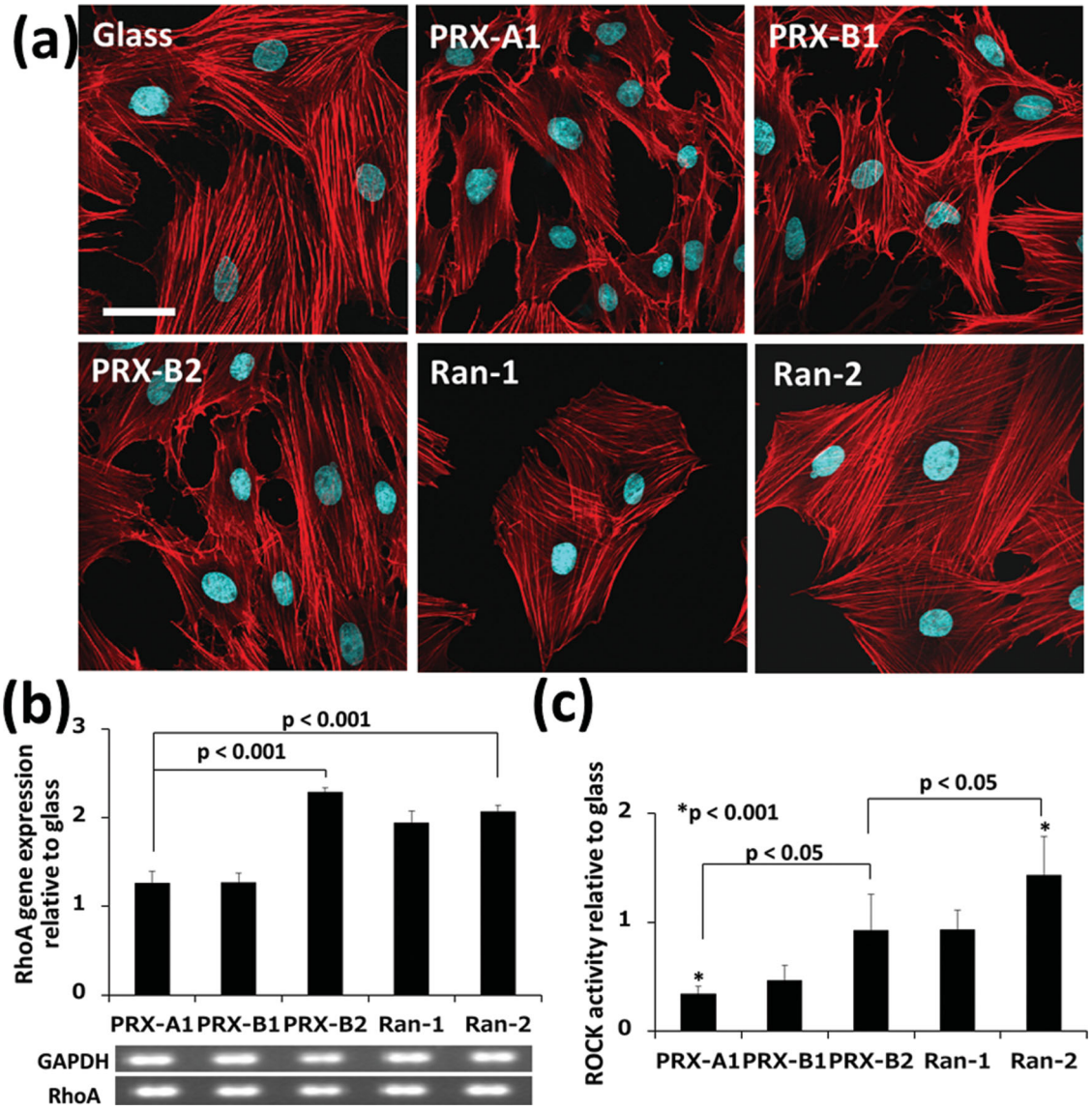

Figure 2. a) Confocal laser microscopy images of MSCs on polymer surfaces. Blue: nuclei, Red: F-actin, Scale bare = 50 μm. b) Relative gene expression level of RhoA, and c) Enzymatic activity of ROCK in adhering MSCs after 4 d of adhesion. Data are presented as mean ± s.d. ($n = 4$), and the results are normalized to that of a glass surface. Optical microscopic images of adhering MSCs are presented in the Supporting Information.

The mechanism underlying the shape dependence of stem cell differentiation is not yet clearly understood. However, several research groups have demonstrated a positive relationship between the expression level of components in the cytoskeletal signaling pathway and the ability to direct MSC lineages.[14] Those studies suggest that the differences in the adhesion morphology affect the expression levels of Ras homolog gene family A (RhoA) and the downstream Rho-associated protein kinase (ROCK) at the initial stage of MSC differentiation. This RhoA-ROCK-mediated signal pathway alters the phosphorylation level of signaling proteins, such as LIM domain kinase (LIMK), resulting in the phosphorylation of cytoskeletal elements, such as cofilin. This signaling pathway feeds back into the determination of the morphology of adherent MSCs, and the expression level of the components in this RhoA-ROCK-mediated communication loop has been proposed to be a molecular switch that is deeply related to the osteogenic or adipogenic differentiation of MSCs.[14a] Therefore, the MSC responses to the different polymer surfaces were further investigated in terms of the gene expression of RhoA and the enzymatic activity of ROCK in adherent MSCs because the RhoA-ROCK-mediated signaling pathway is related to MSC lineage (Figure 2b,c). The results indicated that the MSCs on the Ran-2 surface (low Mf) showed a high level of RhoA gene expression and the highest level of ROCK activity. The MSCs on the PRX-B2 surface (medium Mf) showed a high level of RhoA gene expression and moderate level of ROCK activity, and those on the PRX-A1 surface (high Mf) showed the lowest level of RhoA gene expression and ROCK activity. In this study, a narrow, protruded, and elongated morphology of adherent MSCs also corresponds to MSCs that show a lower level of ROCK activity.

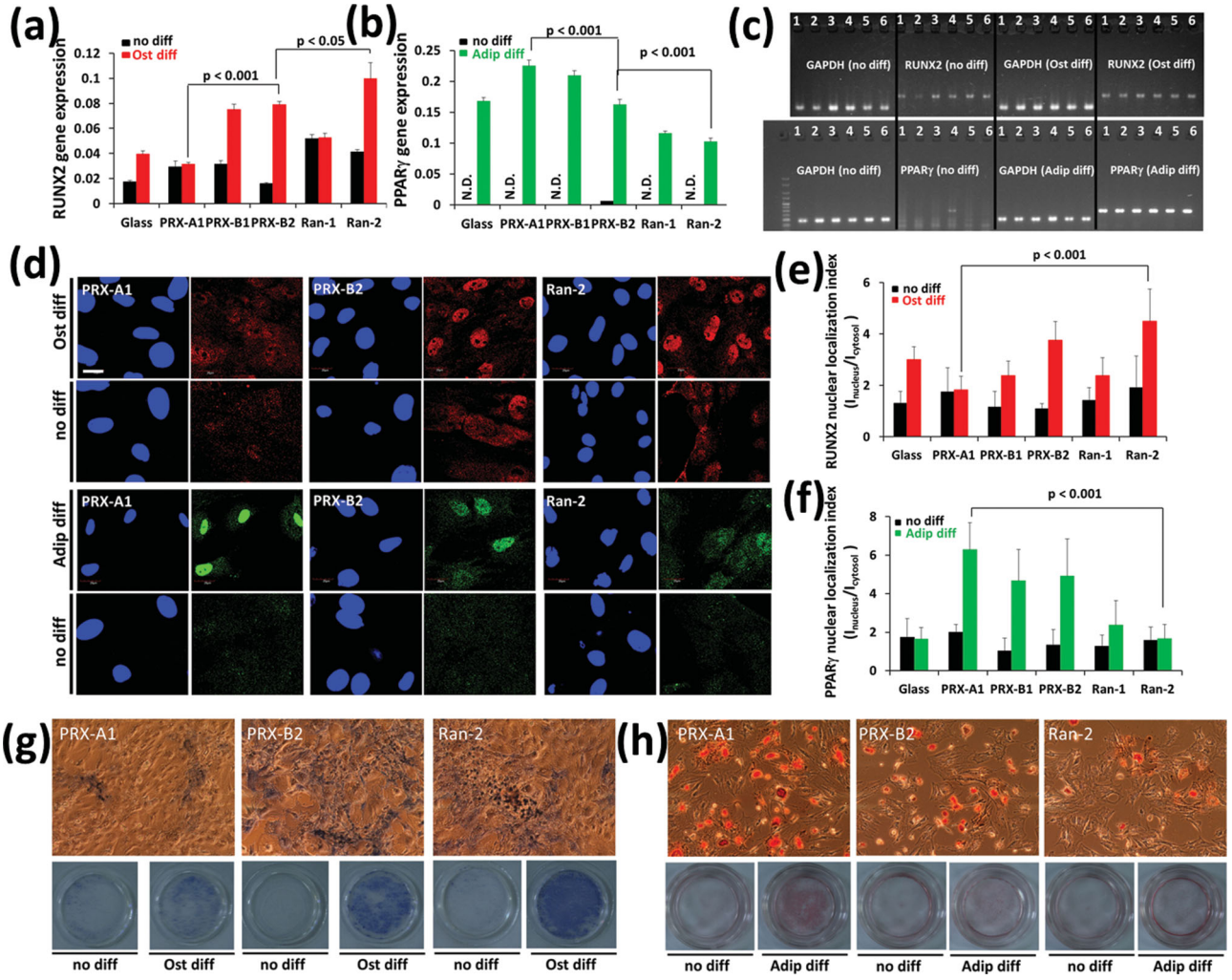

Figure 3. Specific gene and protein expression in the differentiated MSCs. Results of real-time RT-PCR measurement for a) osteogenic (RUNX2) and b) adipogenic (PPARγ) genes after the differentiation into osteogenic and adipogenic cells, respectively. Data are presented a value of $2^{-\Delta CT}$ as mean ± s.d. ($n = 4$). c) The electrophoresis gel images of the resulting genes. The gels are marked with the following numbers — 1: bare glass, 2: PRX-A1, 3: PRX-B1, 4: PRX-B2, 5: Ran-1, and 6: Ran-2. d) Confocal laser microscopic images of osteogenic and adipogenic differentiated MSCs on each polymer. Blue: nucleus, Red: RUNX2. Green: PPARγ, Scale bare = 20 μm. Nuclear localization of e) RUNX2 and f) PPARγ calculated by the pixel inspecting method using ImageJ ($n = 10$). The results for PRX-B1 and Ran-1 are presented in the Supporting Information. g) Results of ALP activity staining of MSCs on PRX-A1, B2, and Ran-2 4 days after differentiation into osteogenic cells. h) Result of Oil Red O staining of MSCs on PRX-A1, B2, and Ran-2 4 d after differentiation into adipogenic cells.

The specific gene expression of adherent MSCs was analyzed 4 d after their differentiation into osteogenic or adipogenic cells. **Figure 3**a,b shows the results of a real-time reverse-transcription polymerase chain reaction (RT-PCR) analysis 4 d post-differentiation. The expression values show the relative level to the expression of house-keeping gene, GAPDH. The relative gene expression level of runt-related transcription factor 2 (RUNX2), which is a marker protein of osteogenic cells, showed the highest value on the Ran-2 surface but a moderate, and the lowest value on the PRX-B2, and A1 surfaces, respectively, when the MSCs differentiated into osteogenic cells. By contrast, the gene expression of peroxisome proliferator-activated receptor-gamma (PPARγ), which is a marker protein of adipogenic cells, showed the highest value on the PRX-A1 surface but a moderate, and the lowest value on the PRX-B2, and Ran-2 surface, respectively, under the condition of adipogenic differentiation.

Figure 3d shows confocal laser microscopic images of adherent MSCs taken after immunostaining of primary antibodies that specifically bind to RUNX2 or PPARγ proteins. The RUNX2 and PPARγ protein expression levels are greatly increased in the nucleus when an external stimulus for osteogenic or adipogenic differentiation is applied to MSCs.[15] Therefore, the protein expression level in the nucleus relative to that in the cytosol is a good index for confirming MSC differentiation at the protein level.[16] Nuclear localization of RUNX2 or PPARγ was observed when the MSCs differentiated into osteogenic or adipogenic cells, respectively. The degree of nuclear localization was calculated using ImageJ analysis, and the results are shown in Figure 3e,f. The nuclear localization

DOI: 10.1002/adhm.201400173

index of RUNX2 was the highest on the Ran-2 surface, while it was the lowest on the PRX-A1 surface. By contrast, the nuclear localization index of PPARγ was highest on the PRX-A1 surface and lowest on the Ran-2 surface.

Histological staining was also conducted to ensure the complete differentiation of the MSCs into osteogenic and adipogenic cells. Figure 3g,h show the alkaline phosphatase (ALP) activity and Oil Red O staining results for adherent MSCs after their differentiation to osteogenic and adipogenic cells, respectively. The MSCs that differentiated on the random copolymer surfaces in the osteogenic medium showed significant positive staining using the ALP staining kit, whereas the MSCs on the PRX block copolymer surfaces showed limited cell staining. In the case of the adipogenic differentiation, numerous lipid vesicles (positively stained for Oil Red O) were found in the MSCs that were cultured on the PRX block copolymer surfaces. However, only a limited number of lipid vesicles could be observed for the MSCs grown on the random copolymer surfaces. The ALP activity and the amount of lipid vesicles were quantitatively analyzed by measuring the enzyme-substrate reaction of ALP and by extracting stained lipid vesicles, respectively. As shown in Figure S8 (Supporting Information), high ALP activity was shown on the Ran-2 surface while the PRX-A1 surface shows the lowest activity. By contrast, a large amount of Oil Red O staining was detected on the PRX-A1 surface, whereas the lowest values were found on the Ran-2 surface (Figure S8, Supporting Information).

Focal adhesion kinase (FAK), which is expressed at focal contacts between integrin and ECM molecules, continuously stabilizes or destabilizes stress fibers for determination of cell morphology.[17] When FAK phosphorylates and activates p190RhoGEF, the RhoA-ROCK-mediated signaling pathway is upregulated, and cytoskeletal tension is promoted by forming stable actin fiber bundles that are cross-linked by α-actinin.[18] Conversely, immature actin fibers are observed when FAK phosphorylates Tyr12 of α-actinin rather than p190RhoGEF (downregulating RhoA-ROCK signaling), thus disrupting the crosslinking of stress fibers. The equilibrium states of the FAK-mediated RhoA-ROCK activation dominate the adhering morphology of cells. Downregulated RhoA-ROCK activity by imbalanced equilibrium induces cell protrusion and elongated morphology while upregulated RhoA-ROCK activity induces spread morphology in various types of cells.[19] We found that the PRX block copolymer surfaces with a higher molecular mobility can easily downregulate the RhoA-ROCK signaling pathway in adherent MSCs, thus resulting in narrow, protruded and elongated morphology with immature stress fibers, as shown in **Figure** 2, S3 (Supporting Information) and **4**b. This up- or downregulated state of the RhoA-ROCK signaling pathway may induce selective MSC differentiation in the present study. Figures 4 and S9 (Supporting Information) show the relationships between the level of ROCK activity and the resulting MSC differentiation tendencies. The RUNX2 gene expression, nuclear localization of the RUNX2 protein, and the corresponding ALP activity increase as the ROCK activity increases, whereas the adipogenic characteristics decrease. Because expression of the RUNX2 gene is characteristic of the early stage of osteogenic differentiation, the expression level of the RUNX2 gene (Figure S9a, Supporting Information) shows a relatively weak dependence on the ROCK activity compared with that of PPARγ 4 d after differentiation. The linear increase or decrease in ALP activity or Oil Red O staining with increasing ROCK activity is clearly observed in Figure 4. Because various reports have suggested that the Rho-ROCK signaling pathway acts as a molecular switch in directing MSCs differentiation into osteogenic or adipogenic cells, this result is well consistent with those reports, and this indicates that the surface molecular mobility is an important physicochemical factor in regulation of ROCK activity for directing stem cell differentiation. In any event, these sets of results indicate that MSCs on the polymer surfaces that are favorable

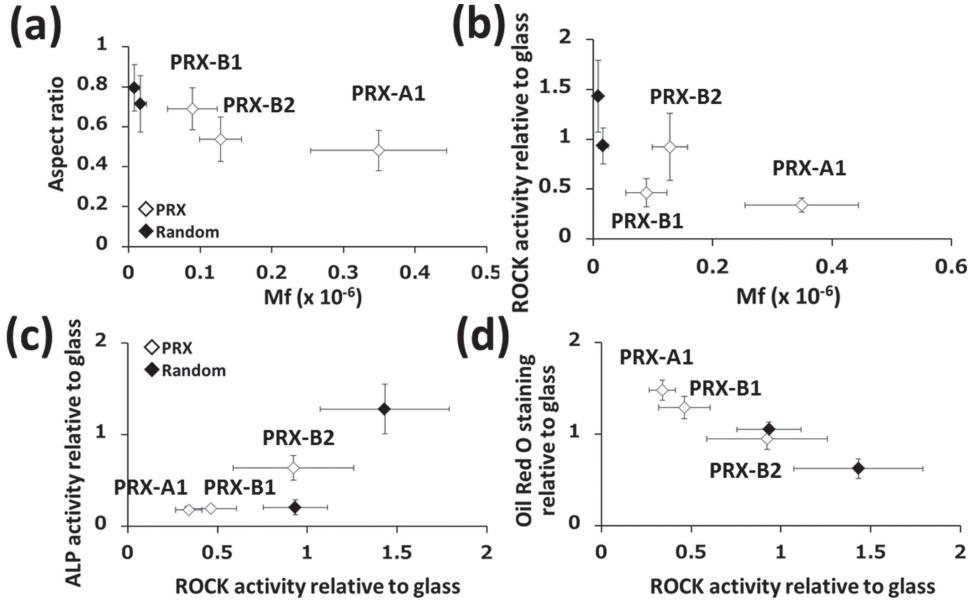

Figure 4. Plot of the a) aspect ratio of the adhering MSCs vs Mf, b) Relative ROCK activity vs RhoA gene expression to glass, and plots of relative ROCK activity against c) ALP activity, and d) amount of Oil Red O staining for the osteogenic and adipogenic differentiation conditions.

ADVANCED HEALTHCARE MATERIALS
www.advhealthmat.de

www.MaterialsViews.com

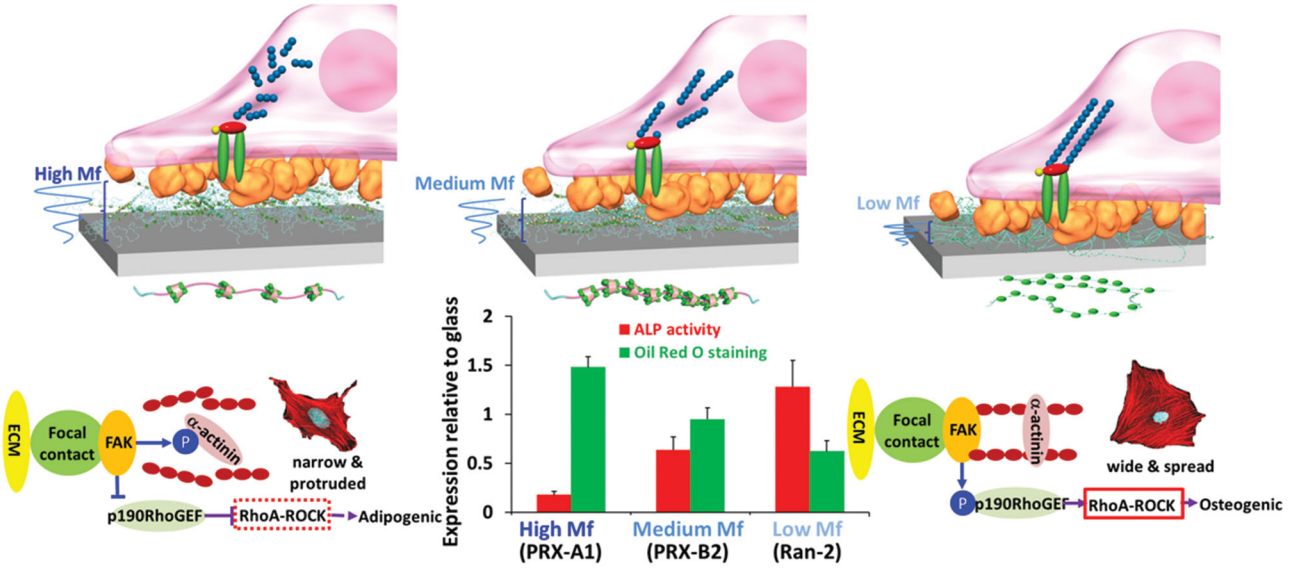

Figure 5. Schematic hypothesis of the different MSCs response to the polymer surfaces and the signaling pathway relating the cytoskeleton to MSC differentiation.

for activating the RhoA-ROCK signaling pathway can easily differentiate into osteogenic cells, whereas the inverse case leads to differentiation into adipogenic cells. The significance of the dynamic nature of cell adhesive surfaces in MSC differentiation has recently attracted much attention. Trappman et al.[20] reported the significant role of the adsorption state of ECM proteins in stem cell differentiation. A tightly tethered collagen matrix on stiff elastomer surfaces activates the extracellular signal-related kinase (ERK)/mitogen-activated protein kinase (MAPK) signaling pathway, leading to the differentiation of MSCs into osteogenic cells. The researchers claimed that the dynamic nature of ECM proteins on the elastomer surface, rather than the stiffness itself, is a dominant factor in determining MSC fate. It has been also suggested that the differentiation of MSCs is also affected by the molecular structure, distribution, or surface density of cell-binding motif on materials surfaces.[21] For that reason, the density of surface fibronectin was analyzed by means of ELISA and the result is listed in Table S2 (Supporting Information). As a result, the difference in fibronectin density on the PRX surfaces was so low to discuss the different tendency of the ALP activity or Oil Red O staining of the differentiated MSCs on the polymer surfaces. This indicates that the difference in MSC differentiation on the PRX surfaces could not be explained in terms of fibronectin density, but the molecular mobility is much more useful to discuss the results. In the case of Ran-1 and Ran-2 surfaces, the degree of ROCK activity and osteogenesis was increased as the surface density of fibronectin. Because there is no significant difference in Mf values between Ran-1 and Ran-2, the difference in osteogenic differentiation on the non-dynamic Ran-1 and Ran-2 is possibly induced by twofold higher fibronectin density on the Ran-2 surface as previous report, i.e., density of cell-binding motif.[21] The further researches are undergoing to clearly understand the relationships between the density of fibronectin and MSC differentiation on the different set of polymer surfaces. However, it is not yet concluded and is out of the scope of the present study. Thus, we hypothesized that fibronectin that is adsorbed on PRX surfaces with high molecular mobility provides loosely tethered cell-binding motifs, inducing immature actin fiber bundles with the subsequent downregulation of RhoA-ROCK activity. Consequently, this downregulation induced by high molecular mobility presumably directs MSCs to differentiate into adipogenic cells, as depicted in **Figure 5**.

Various types of materials have been designed to effectively regulate the fate of stem cells. A simple surface deposition method that does not alter bulk properties and is capable of regulating stem cell lineage provides great potential in various biomedical applications, such as implant materials or sensor surfaces. Thus, the potential utility of simple polymer deposition as a molecular platform for directing stem lineage was examined. Adopting the threaded macromolecular PRX platform could allow for the production of polymer surfaces with wide range of molecular mobility to regulate the RhoA-ROCK signaling pathway of MSCs and easily regulate stem cell fate.

Experimental Section

Preparation of the Polymer Surfaces: All the PRX and random copolymers were prepared as previously reported.[6] The copolymers (5 mg) were initially dispersed in 5 mL of ethanol, and then 5 mL of deionized water was added to prepare 0.05 wt% clear copolymer solutions. Each copolymer solution (100 μL) was cast on a glass-bottomed dish ($\varphi = 27$ mm; Iwaki Glass, Tokyo, Japan) and was naturally dried in a clean box. The dried polymer surfaces were stabilized in water for 1 h for the subsequent applications.

Calculation of the Viscoelastic Factor (Mf) in a Hydrated State Using QCM-D Analysis: The viscoelastic factor of the polymer surfaces in hydrated states was analyzed by means of a QCM-D measurement (Q-sense E1-HO, Gothenburg, Sweden) as a previously reported method with the following equation.[6] The details are explained in the Supporting Information.

DOI: 10.1002/adhm.201400173

$$Mf = (D_{polymer,wet} - D_{SiO2,wet}) / (f_{SiO2,dry} - f_{polymer,dry})$$

Isolation of Rat MSCs: The animal experiment was performed in compliance with the guidelines of the Biosafety Committee at National Cerebral and Cardiovascular Center Research Institute. Rat bone-marrow-derived MSCs were isolated from 4-week-old male Fischer 344 rats (NSlc, weights: 50–70 g, Japan SLC Co., Hamamatsu, Japan). The thighbone and tibia were flushed with alpha MEM (Gibco Invitrogen Corp., Grand Island, NY, USA) supplemented with 10% fetal bovine serum, 1% penicillin/streptomycin, and 1% heparin to extract the bone marrow. The cell suspension was then passed through a 40-μm cell strainer (BD Falcon, Franklin Lakes, NJ, USA) and centrifuged (1500 rpm, 3 min). The precipitate was suspended in fresh medium without heparin, centrifuged, and resuspended in fresh medium for cell culture. After a 24 h incubation, the cultured cells were washed with fresh medium to remove non-adherent cells, and the medium was changed every 24 h until the cultured cells proliferated to approximately 80% confluence. The proliferated cells were detached with a 0.05% trypsin-EDTA solution and directly used for the following experiments.

Cell Culture and Differentiation of MSCs on the Polymer Surfaces: Each polymer surface was brought into contact with 10 μg mL^{-1} of human fibronectin solution (F0003; Asahi Glass Co., Ltd., Tokyo, Japan) for 1 h at 37 °C. After a rinse with phosphate-buffered saline (PBS, pH 7.4; Gibco Invitrogen Corp.), 1.2×10^5 cells were cultured on each polymer surface. After a 4 h incubation, the non-adherent MSCs were removed by gentle washing with PBS, and the medium was changed to either osteogenic or adipogenic differentiation medium (StemPro-MSC differentiation medium; Gibco Invitrogen Corp.). In the case of non-differentiation, the medium was changed to a control medium (StemProSFM for MSC; Gibco Invitrogen Corp.).

Evaluation of the Morphology of Adherent MSCs and ROCK Activity: After 4 d of incubation in non-differentiation medium, the adherent MSCs were washed with fresh PBS and fixed with 4.0% formaldehyde for 15 min at room temperature. After being washed with fresh PBS, the cells were permeabilized with 1.0% Triton X-100 for 5 min and rinsed again with PBS. Rhodamine-conjugated phalloidin (Invitrogen Corp.) was diluted as directed by the manufacturer and allowed to react with fixed MSCs in the dark for 1 h at room temperature. The samples were then washed with PBS and mounted with ProLong gold antifade reagent containing DAPI (Invitrogen Corp.) prior to confocal laser microscopy (FV10i, Olympus, Tokyo, Japan). The projected cell area and best-fit ellipse aspect ratio of the stained MSCs were calculated using ImageJ (v. 1.47, National Institutes of Health, Bethesda, MD, USA). More than 10 standard MSC images were analyzed for each sample, and the aspect ratio was used in inverse form, that is, short axis divided by the long axis. To evaluate ROCK activity in adherent MSCs, the total protein of the adherent MSCs (4 d, non-differentiated) was extracted using a Minute detergent-free protein extraction kit (Invent Biotechnologies Inc., Eden Prairie, MN, USA) per the manufacturer's instructions, and the concentration of the extracted protein was calculated using a micro-BCA (Thermo Fisher Scientific, Waltham, MA, USA) protein assay kit with bovine serum albumin-based calibration. The concentration of the total protein solution was adjusted to 10 ng μL^{-1}, and the solution was immediately tested using an enzyme-linked immunosorbent assay (ELISA) kit (STA-416, Cell Biolabs Inc., San Diego, CA, USA) to measure the ROCK activity according to the manufacturer's instructions.

Quantitative Real-Time RT-PCR Analysis of Adherent MSCs: After 4 d incubation, 2.0 μg of the total RNA of non-differentiated (for RhoA) or differentiated (for RUNX2 and PPARγ) MSCs was isolated using a PureLink RNA Mini kit (Ambion Life Technologies, Carlsbad, CA, USA). The isolated total RNA was then reverse transcribed using a cDNA reverse transcription kit (Applied Biosystems, Darmstadt, Germany). PCR was conducted with 50 ng (4 μL) of cDNA with 25 μL of SYBR real-time PCR master mix (Toyobo, Osaka, Japan) and 2.0 μL of forward and reverse primer mix (25×10^{-6} M). All primers were purchased from Sigma–Aldrich Chemical Co. (St. Louis, MO, USA), and the sequences are listed below. The cycling conditions were as follows: 95 °C for 2 min, followed by 40 cycles of 95 °C for 20 s, 55 °C for 30 s, and 68 °C for 30 s. The resulting single band of the PCR mixture was then confirmed using 2% agarose gel electrophoresis, which was stained with ethidium bromide, followed by UV visualization. The expression level of the marker gene was normalized to the GAPDH level and calculated with the $2^{-\Delta\Delta CT}$ formula.[22] All values were normalized to the expression level on the bare glass surface for discussion.

Primer Sequences: GAPDH (forward: 5′-GACATGCCGCCTGGAGAAAC-3′, reverse: 5′-AGCCCAGGATGCCCTTTAGT-3′), RUNX2 (forward: 5′-GCCG-GGAATGATGAGAACTA-3′, reverse: 5′-TTGGGGAGGATTTGTGAAGA-3′), PPARγ (forward: 5′-CCTTTACCACGGTTGATTTCTC-3′, reverse: 5′-GGCTCTACTTT-GATCGCACTTT-3′), and RhoA (forward: 5′-ACTGGTGATTGTTGGTGATGGAGC-3′, reverse: 5′-TGGGCACATAAACCTCTGGGAAC-3′).[23]

Immunostaining of RUNX2 and PPARγ Proteins: After 4 d of differentiation, the adherent MSCs were rinsed with PBS and fixed with 4.0% formaldehyde for 15 min at room temperature. The MSCs were then rinsed with PBS and permeabilized with 1.0% Triton-X100 for 5 min at room temperature. The samples were immersed in blocking solution consisting of PBS with 5.0% goat serum and 0.30% Triton X-100 for 1 h at room temperature and allowed to react with the primary antibody [mouse anti-RUNX2 monoclonal antibody (ab76956, Abcam, Cambridge, UK) or rabbit PPARγ monoclonal antibody (C26H12; Cell Signaling Technology, Danvers, MA, USA)] for 12 h at 4 °C. After being washed with PBS three times, the samples were allowed to react with the secondary antibody [goat anti-mouse IgG H/L Alexa555 (ab150114, Abcam) or goat anti-rabbit IgG H/L Alexa488 (4412S, Cell Signaling Technology)] for 1 h in the dark. After three rinses with PBS, the samples were mounted with ProLong gold antifade reagent containing DAPI for confocal laser microscopy. The nuclear localization index ($I_{nucleus}/I_{cytosol}$) of RUNX2 and PPARγ was calculated using the pixel inspection tool in ImageJ. More than three pixel regions (7×7) were averaged for the nucleus and for the cytosol, and estimates were made using more than 10 standard MSC images for statistical analysis.

ALP Activity and Oil Red O Staining: The ALP activity and Oil Red O staining of differentiated osteogenic or adipogenic MSCs were measured using an ALP staining kit (AK20) and a lipid assay kit (AK09F) purchased from Cosmo Bio Co., Ltd. (Tokyo, Japan), respectively. Briefly, differentiated MSCs were rinsed with PBS and fixed with 4.0% formaldehyde. After a rinse with fresh PBS, the samples were allowed to react with the corresponding staining kit at 37 °C for 10 min, followed by a rinsing and drying process. The amount of Oil Red O staining was analyzed by isolating the stained lipids using an extraction kit (AK20) according to the manufacturer's instructions. ALP activity was quantitatively determined by reacting the cell lysates with *p*-nitro-phenyl phosphate per the manufacturer's instructions (MK301, Takara Bio Inc., Shiga, Japan).

Supporting Information

Supporting Information is available from the Wiley Online Library or from the author.

Acknowledgements

Part of this research was financially supported by a Grant-in-Aid for Scientific Research B [No. 25282142, Japan Society for the Promotion of Science (JSPS)]. Isolation of MSCs from rat was approved by the Biosafety Committee at National Cerebral and Cardiovascular Center Research Institute.

Received: March 31, 2014
Revised: June 18, 2014
Published online:

[1] A. I. Caplan, *J. Orthop. Res.* **1991**, *9*, 641.
[2] a) E. S. Place, N. D. Evans, M. M. Stevens, *Nat. Mater.* **2009**, *8*, 457; b) A. H. Ambre, D. R. Katti, K. S. Katti, *J. Biomed. Mater. Res.* **2013**, *101*, 2644; c) A. F. Steinert, L. Rackwitz, F. Gilbert, U. Noth, R. S. Tuan, *Stem Cells Trans. Med.* **2012**, *1*, 237; d) O. Guillaume-Gentil, O. V. Semenov, A. H. Zisch, R. Zimmermann, J. Voros, M. Ehrbar, *Biomaterials* **2011**, *32*, 4376.
[3] A. J. Engler, S. Sen, H. L. Sweeney, D. E. Discher, *Cell* **2006**, *126*, 677.
[4] F. Guilak, D. M. Cohen, B. T. Estes, J. M. Gimble, W. Liedtke, C. S. Chen, *Cell Stem Cell* **2009**, *5*, 17.
[5] a) N. Huebsch, P. R. Arany, A. S. Mao, D. Shvartsman, O. A. Ali, S. A. Bencherif, J. Rivera-Feliciano, D. J. Mooney, *Nat. Mater.* **2010**, *9*, 518; b) S. Khetan, M. Guvendiren, W. R. Legant, D. M. Cohen, C. S. Chen, J. A. Burdick, *Nat. Mater.* **2013**, *12*, 458; c) K. Kolind, K. W. Leong, F. Besenbacher, M. Foss, *Biomaterials* **2012**, *33*, 6626.
[6] a) J.-H. Seo, S. Kakinoki, Y. Inoue, T. Yamaoka, K. Ishihara, N. Yui, *Soft Matter* **2012**, *8*, 5477; b) J.-H. Seo, N. Yui, *Biomaterials* **2013**, *34*, 55.
[7] a) J.-H. Seo, S. Kakinoki, Y. Inoue, K. Nam, T. Yamaoka, K. Ishihara, A. Kishida, N. Yui, *Biomaterials* **2013**, *34*, 3206; b) J.-H. Seo, S. Kakinoki, Y. Inoue, T. Yamaoka, K. Ishihara, N. Yui, *J. Am. Chem. Soc.* **2013**, *135*, 5513.
[8] S. Kakinoki, J.-H. Seo, Y. Inoue, K. Ishihara, N. Yui, T. Yamaoka, *J. Biomater. Sci. Polym. Ed.* **2013**, *24*, 1320.
[9] N. J. Hallab, K. O' Connor, R. L. Moses, J. J. Jacobs, *Tissue Eng.* **2001**, *7*, 55.
[10] D. A. Lamprou, J. R. Smith, T. G. Nevell, E. Barbu, C. Stone, C. R. Willis, J. Tsibouklis, *Appl. Surf. Sci.* **2010**, *256*, 5082.
[11] a) N. Ishida, S. Biggs, *Langmuir* **2007**, *23*, 11083; b) A. Naderi, P. M. Claesson, *Langmuir* **2006**, *22*, 7639.
[12] G. Fleury, C. Brochon, G. Schlatter, G. Bonnet, A. Lapp, G. Hadziioannou, *Soft Matter* **2005**, *1*, 378.
[13] J. P. Rodriguez, M. Gonzalez, S. Rios, V. Cambiazo, *J. Cell Biochem.* **2004**, *92*, 721.
[14] a) R. McBeath, D. M. Pirone, C. M. Nelson, K. Bhadriraju, C. S. Chen, *Dev. Cell* **2004**, *6*, 483; b) Y. K. Wang, X. Yu, D. M. Cohen, M. A. Wozniak, M. T. Yang, L. Gao, J. Eyckmans, C. S. Chen, *Stem Cells Dev.* **2012**, *21*, 1176.
[15] W. Zou, M. B. Greenblatt, N. Brady, S. Lotinun, B. Zhai, H. de Rivera, A. Singh, J. Sun, S. P. Gygi, R. Baron, L. H. Glimcher, D. C. Jones, *J. Exp. Med.* **2013**, *210*, 1793.
[16] K. A. Kilian, B. Bugarija, B. T. Lahn, M. Mrksich, *Proc. Natl. Acad. Sci.* **2010**, *107*, 4872.
[17] S. K. Mitra, D. A. Hanson, D. D. Schlaepfer, *Nat. Rev. Mol. Cell Biol.* **2005**, *6*, 56.
[18] J. Zhai, H. Lin, Z. Nie, J. Wu, R. Canete-Soler, W. W. Schlaepfer, D. D. Schlaepfer, *J. Biol. Chem.* **2003**, *278*, 24865.
[19] a) E. A. Cox, S. K. Sastry, A. Huttenlocher, *Mol. Biol.* **2001**, *12*, 265; b) G. Totsukawa, Y. Wu, Y. Sasaki, D. J. Hartshorne, Y. Yamakita, S. Yamashiro, F. Matsumura, *J. Cell Biol.* **2004**, *164*, 427.
[20] B. Trappman, J. E. Gautrot, J. T. Connelly, D. G. T. Strange, Y. Li, M. L. Oyen, M. A. Cohen Stuart, H. Boehm, B. Li, V. Vogel, J. P. Spatz, F. M. Watt, W. T. S. Huck, *Nat. Mater.* **2012**, *11*, 642.
[21] K. A. Kilian, M. Mrksich, *Angew. Chem.* **2012**, *124*, 4975.
[22] a) K. J. Livak, T. D. Schmittgen, *Methods* **2001**, *25*, 402; b) T. D. Schmittgen, K. J. Livak, *Nat. Protoc.* **2008**, *3*, 1101.
[23] Y. Wang, X. Jiang, S. Yang, X. Lin, Y. He, C. Yan, L. Wu, G. Chen, Z. Wang, Q. Wu, *Biomaterials* **2011**, *32*, 9207.

Adv. Healthcare Mater. **2014**,
DOI: 10.1002/adhm.201400173